Single Crystal Growth of Sillén–Aurivillius Perovskite Oxyhalides Bi$_4$NbO$_8$X (X = Cl, Br)

Chengchao Zhong [1], **Daichi Kato** [1] (ID), **Fumitaka Takeiri** [1] (ID), **Kotaro Fujii** [2], **Masatomo Yashima** [2], **Emily Nishiwaki** [1], **Yasuhiro Fujii** [3] (ID), **Akitoshi Koreeda** [3], **Cédric Tassel** [1], **Ryu Abe** [1,4,*] and **Hiroshi Kageyama** [1,4,*] (ID)

[1] Department of Energy and Hydrocarbon Chemistry, Graduate School of Engineering, Kyoto University, Nishikyo-ku, Kyoto 615-8510, Japan; shou.shouchou.26m@st.kyoto-u.ac.jp (C.Z.); kato.daichi.54c@st.kyoto-u.ac.jp (D.K.); f.takeiri@gmail.com (F.T.); emn41@case.edu (E.N.); cedric.tassel@gmail.com (C.T.)

[2] Department of Chemistry, School of Science, Tokyo Institute of Technology, Tokyo 152-8551, Japan; kfujii@cms.titech.ac.jp (K.F.); yashima@cms.titech.ac.jp (M.Y.)

[3] Department of Physical Sciences, Ritsumeikan University, Kusatsu, Shiga 525-8577, Japan; yfujii@fc.ritsumei.ac.jp (Y.F.); kore@fc.ritsumei.ac.jp (A.K.)

[4] CREST, Japan Science and Technology Agency (JST), Kawaguchi, Saitama 332-0012, Japan

* Correspondence: ryu-abe@scl.kyoto-u.ac.jp (R.A.); kage@scl.kyoto-u.ac.jp (H.K.); Tel.: +81-075-383-2478 (R.A.); +81-075-383-2506 (H.K.)

Abstract: Sillén–Aurivillius perovskite Bi$_4$NbO$_8$X (X = Cl, Br) is a promising photocatalyst for water splitting under visible light, as well as a potential ferroelectric material. In this work, we investigate the crystal growth conditions by mainly varying soak temperature, soak time and cooling rate. Under the optimal conditions, we successfully obtained yellow platelet single crystals with an in-plane distance of several hundred microns. As opposed to conventional crystal growth, a moderate cooling is essential to suppress an evaporation of the Bi–O–Cl species from a melt zone. The single crystals of Bi$_4$NbO$_8$Br were also grown using a similar condition. We suggest that the knowledge obtained in this study can be generally applied to other Sillén–Aurivillius phases and related oxyhalides.
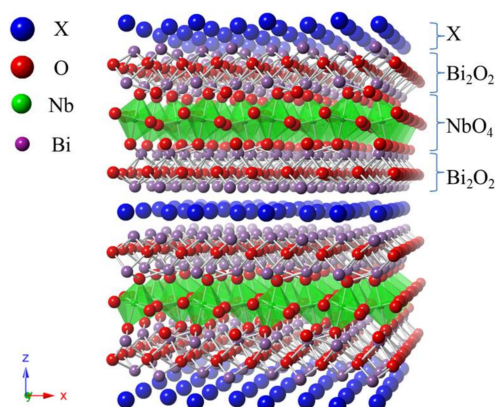
1. Introduction

Mixed-anion compounds, where multiple anions are present in a single component, show novel physical and chemical functions that are not accessible in single oxide materials. These functions arise from differing anionic characters such as formal charge, polarizability, and electronegativity [1–3]. A representative example is visible-light driven photocatalysts for water splitting, where non-oxide anions with less electronegativity leads to the reduction of band gap relative to corresponding oxides [4–7]. Except for a few examples [4], however, stable photocatalytic activity has not been achieved, mainly because of self-decomposition of catalysts by photo-generated holes near valence band maximum.

We have recently reported that layered oxyhalides Bi$_4$NbO$_8$X (X = Cl, Br) can split water stably and efficiently under visible light irradiation [8]. Bi$_4$NbO$_8$Cl, originally synthesized and structurally characterized by Ackerman [9], belongs to Sillen–Aurivillius type layered perovskite (space group: $P2_1cn$) with single perovskite NbO$_4$ layers sandwiched by double Bi$_2$O$_2$ layers and a single halide X layer along the c axis (Figure 1). What makes Bi$_4$NbO$_8$X distinct from other mixed-anion photocatalysts is the fact that the valence band maximum is predominantly occupied by oxygen 2p-orbitals. The

unusual valence band structure is accounted for by the electrostatic destabilization of oxide $2p$ orbitals [10] as well as the hybridization between Bi $6s$ and O $2p$ orbitals [11].

Figure 1. Crystal structure of Sillén–Aurivillius type perovskite Bi_4NbO_8X (X = Cl, Br). The purple, red and blue balls denote Bi, O and X atoms, respectively. Nb-centered octahedra are shown in green.

In order to obtain further insight into the photocatalytic properties of Bi_4NbO_8X, such as carrier dynamics of photo-generated holes and electrons, the measurements using single crystals are desirable. Ackerman obtained single crystal Bi_4NbO_8Cl by a simple melt growth technique [9]; a sintered Bi_4NbO_8Cl in an alumina crucible was sealed into an evacuated silica tube, heated to 1150 °C, kept for 5 h and cooled to room temperature at a rate of 10 °C/h. However, without any reason, a large amount of sample (1 kg) was used, which is hard to apply to a lab-scale experiment. Moreover, little information on the obtained single crystals (e.g., size and morphology) was given. Thus, one only knows that the crystal size was large enough for structural determination with single-crystal X-ray diffraction (XRD) [9].

Mixed-anion compounds often encounter difficulties in forming a melt zone when anionic species have differing volatilities. In the present case, we can deduce a difficulty of forming a stable melt zone because of the volatility of BiOX (X = Cl, Br). In fact, BiOX can be grown by vapor transport technique [12,13], and also used as a transport agent (BiOX(s) + H_2O(g) ↔ Bi(H_2O)$_2$X) [14]. In this study, we devote our attention to optimum conditions for growing single crystals of Bi_4NbO_8Cl and Bi_4NbO_8Br by mainly varying soak temperature, soak time and cooling rate.
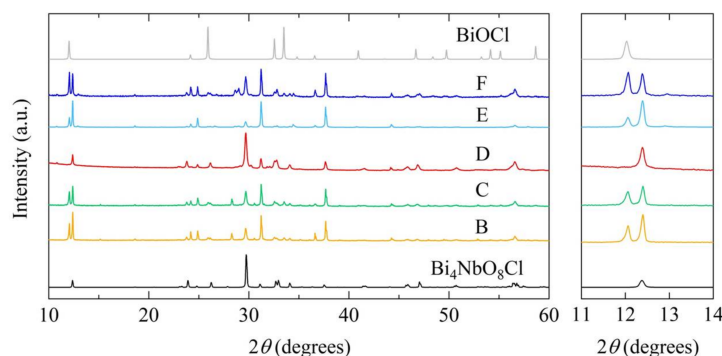
2. Results and Discussion

2.1. Growth Condition of Bi_4NbO_8Cl
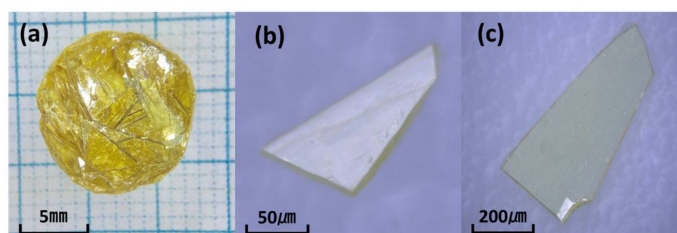
We initially attempted to grow Bi_4NbO_8Cl single crystals by simply scaling-down the growth conditions reported to the scale of 1 kg [9]. Bi_4NbO_8Cl powder (4 g) prepared by the conventional solid state reaction was heated at 1150 °C for 5 h, followed by the cooling down to 25 °C at the rate of 10 °C/h (Condition A in Table 1). We observed grey agglomerate at the alumina tube bottom without any crystal-like particles, while some transparent platelet crystals (approx. 2 mm × 2 mm) were adhered to the upper part of the tube. Powder XRD for both products in crushed powder form revealed that the grey agglomerate is composed of Bi_4NbO_8Cl, BiOCl and $BiNbO_4$ with the refined molar ratio of 21:24:55, while the transparent platelet crystals are entirely BiOCl (Figure S1). These observations suggest that there is a continuous loss of Bi–O–Cl species from the melt as a vapor, leading to nucleation and growth of BiOCl crystals. Hence, we decided to lower a soak temperature (1075 °C) to prevent the Bi–O–Cl volatilization.

Table 1. Conditions for single crystal growth of Bi_4NbO_8Cl.

Samples	Soak Temperature (°C)	Soak Time (h)	Cooling Rate (°C/h)	Slow Cooling Temperature (°C)
A	1150	5	10	25
B	1075	5	2	875
C	1075	5	5	875
D	1075	5	10	875
E	1075	10	10	875
F	1075	20	10	875

Figure 2. Powder X-ray diffraction (XRD) of the products obtained from different conditions (B–F) listed in Table 1. The top and bottom XRD data represent BiOCl [15] and Bi_4NbO_8Cl [16], respectively simulated from the ICSD database. The right panel is enlarged view of 2θ = 11–14°. 2θ = 12.0° belongs to the 001 reflection of BiOCl and 2θ = 12.3° is the 004 reflection of Bi_4NbO_8Cl.

We also found that the cooling rate is important. As opposed to conventional cases where a slower cooling rate is encouraged to obtain crystals of high quality [17,18], a slower cooling rate resulted in the volatilization of Bi–O–Cl species; at a cooling rate of 2 °C/h and 5 °C/h (Condition B and C), we observed grey agglomerate (4 mm in height) on top of yellow crystalline mass (3 mm in height), as shown in Figure S2. The BiOCl single crystals were found on the walls of the crucible and on the surface of the grey agglomerate. We picked up serveral crystals from the yellow crystalline mass and measured their powder XRD (Figure 2), revealing multiple phases attributed to Bi_4NbO_8Cl, BiOCl and $BiNbO_4$. In contrast, when the cooling rate of 10 °C/h (Condition D) was employed, we observed only a bright yellow mass of crystals with clear facets (Figure 3a). In addition, powder XRD patterns of the crushed crystals showed a single phase of Bi_4NbO_8Cl (Figure 2). No BiOCl crystals were found on the walls of the crucibles.

Figure 3. (**a**) The obtained crystalline mass; (**b**) A $120 \times 80 \times 20$ μm^3 crystal stripped from crystalline mass; (**c**) A $340 \times 210 \times 40$ μm^3 crystal consisting of two domains superimposed along the *c* axis.
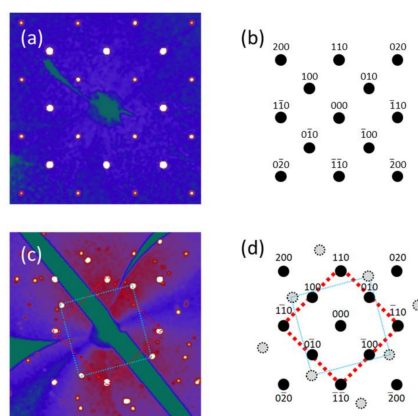
From these results, it can be proposed that the suppression of Bi–O–Cl loss from the melt is crucial. As naturally expected, the soak time also provides a large influence on the products formed: the soaking time of both 10 h and 20 h at 1075 °C (Condition E and F) resulted in the loss of Bi–O–Cl

species, forming BiOCl single crystals outside the melt zone (see Figure 2). We deduce that the use of 1 kg sample in Ref. [9] caused the generation of a sizable Bi–O–Cl vapor pressure, which suppressed a Bi–O–Cl loss from the melt zone at 1150 °C.

2.2. Characterization of Bi_4NbO_8Cl

Unless otherwise specified, we hereafter characterize the Bi_4NbO_8Cl crystals obtained in the optimized condition (Condition D). The energy-dispersive X-ray spectroscopy (EDX) spectra of a single crystal (based on inspection of 12 points) show an average elemental distribution of Bi:Nb:Cl = 0.26:0.06:0.06 (Figure S3a), in accordance with the nominal molar ratio of 4:1:1 for Bi_4NbO_8Cl. A single-crystal XRD measurement was conducted for a platelet crystal of approx. $120 \times 80 \times 20$ μm^3 (Figure 3b). All the in-plane (*ab* plane) spots can be indexed as shown in Figure 4a,b. The refinement in the space group $P2_1cn$ provided the lattice parameters of $a = 5.4835(3)$ Å, $b = 5.4850(3)$ Å, $c = 28.682(2)$ Å, along with $R_1 = 0.0374$, w$R_2 = 0.1000$. The atomic positions and isotropic thermal parameters for Bi_4NbO_8Cl are listed in Table S1 while the interatomic distances and angles are given in Table S2.

The structure of Bi_4NbO_8Cl was precisely refined by Lightfoot and his coworkers by using powder neutron data (space group: $P2_1cn$, $a = 5.4472(1)$ Å, $b = 5.4901(1)$ Å, $c = 28.8125(6)$ Å) [16]. As compared with the single-crystal work that yielded unusual bond valence sum values, e.g., 5.23 and 1.20 for Bi(3) and O(8), respectively [9], our refinement shows reasonable atomic positions as well as the bond valence sum, as shown in Table S3. However, the in-plane parameters in our study and Ref. [9] are very close, indicating the obtained crystal is actually a pseudo-merohedral twin with domains existing along a four-fold axis. The formation of the pseudo-merohedral twin may cause a certain deviation of the O positions from the powder neutron data [16].

Figure 4. Reciprocal lattice plane of Bi_4NbO_8Cl along [001] direction for a crystal of (**a**) 120 μm × 80 μm × 20 μm (Figure 3b) and (**c**) 340 μm × 210 μm × 40 μm (Figure 3c) indexed with the $P2_1cn$ cell as shown in (**b**) and (**d**), respectively.

A larger crystal of 340 μm × 210 μm × 40 μm (Figure 3c) was also chosen for single crystal XRD analysis. When viewed along the *c* direction (Figure 4c), some redundant spots are observed which can be indexed by the superimposition of two different single crystals rotated along [001] (Figure 4d).

2.3. Polarized Raman Measurement of Bi_4NbO_8Cl

Figure 5a shows the results of parallel polarized Raman measurements obtained in parallel nicol geometries in a spectral range from 0 to 1000 cm^{-1} at θ = 0°, 45°, 90°, where θ shows the incident polarization-direction with respect to the crystallographic [100] or [010] axis. From the point symmetry of Bi_4NbO_8Cl (*mm*2), the Raman active modes are A$_1$(z), A$_2$, B$_1$(x) and B$_2$(y). The angular dependence of Raman intensity is shown in Figure 5b. Here, we focus our attention on the representative peaks at 249.6 cm^{-1} and 485.5 cm^{-1}, whose integrated intensities are shown in Figure 5c. Since the former

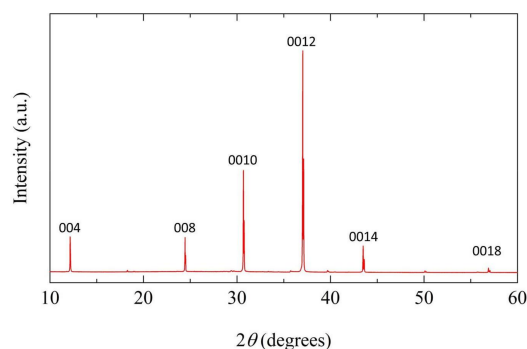takes maxima at θ = 0°, 90°, 180°, this mode is assigned to be $A_1(z)$ symmetry. In contrast, the latter is assigned to be A_2 symmetry. The angular dependence of integrated intensity is shown in Figure 5b,c. It can be found that the intensity of $A_1(z)$ mode varies with the angles, with equal intensity obtained at 0° and 90°. This originates from the similar lattice parameters of *a* and *b* with close relation to pseudo-tetragonal structure. The angular dependence of depolarized Raman spectrum in a cross-nicol polarized geometry (Figure S4) shows that $A_1(z)$ modes also have equal intensity at 0° and 90°. The detailed analysis along with the temperature dependence will be discussed elsewhere.

Figure 5. (**a**) Raman spectra in parallel nicol geometries obtained in a spectral range from 0 to 1000 cm^{-1}; (**b**) Contour plots of angular dependences of the polarized Raman intensity; (**c**) Angular dependence of the integrated Raman intensities of the modes at 249.6 cm^{-1} and 485.5 cm^{-1} indicated by vertical red and pink lines in (**c**). These modes are assigned to be $A_1(z)$ and A_2 modes respectively.

2.4. Single Crystal Growth of Bi_4NbO_8Br

A report on the single crystal growth of Bi_4NbO_8Br is absent to date. We applied the optimized growth condition (Condition D) to the oxybromide and successfully obtained a yellow crystal aggregate of single crystals with clear facets as found in Bi_4NbO_8Cl. No BiOBr single crystal was formed on the tube, indicating that the volatilization of Bi–O–Br species was suppressed. The EDX study of a crystal (75 × 60 × 20 μm^3, Figure S3b) revealed the molar ratio Bi:Nb:Br = 4:1:1, while the powder XRD on the crushed single crystals yielded *a* = 5.4711(4) Å, *b* = 5.5249(3) Å and *c* = 29.1206(5) Å (Figure 6), in agreement with earlier powder neutron refinement [19]. The single crystal XRD profiles of this crystal are indexed as shown in Figure S5. The atomic positions and isotropic thermal parameters for Bi_4NbO_8Br are listed in Table S4 while the interatomic distances and angles are given in Table S5. However, the in-plane lattice parameter is almost equal with *a* = 5.51190(10) Å, *b* = 5.51190(10) Å and *c* = 29.0984(14) Å, suggesting that the obtained platelet crystal is also a pseudo-merohedral twin as was found in Bi_4NbO_8Cl.

Figure 6. Powder XRD pattern of crushed Bi_4NbO_8Br single crystals, showing a strong orientation to the *c* axis.

3. Materials and Methods

3.1. Crystal Growth

As-received powders of Bi_2O_3 (Wako, 99.99%, Osaka, Japan), BiOCl (Wako, 99.5%, Osaka, Japan), Nb_2O_5 (Wako, 99.9%, Osaka, Japan) were used as the starting materials. BiOBr was prepared with a soft liquid deposition method [20]. Reagents weighed according to the stoichiometric ratio were mixed in an agate mortar, put into an alumina Tammann tube (inner diameter 13 mm, 8 cm in length; Nikkato, Osaka, Japan), and then sealed into an evacuated silica tube (inner diameter 15 mm, ca. 15 cm in length; Hayashi-factory, Kyoto, Japan). The tube was put in an electric furnace (NHK-170, Nitto Kagaku, Nagoya, Japan) and heated at 1150 °C or 1075 °C in a heating rate of 200 °C/h in order to form a melt. After maintaining the temperature for 5 h, 10 h and 20 h, the furnace was cooled to 875 °C at a rate of 2 °C/h, 5 °C/h and 10 °C/h, followed by a faster cooling (30–50 °C/h) down to room temperature, as summarized in Table 1.

3.2. Characterizations

The powder XRD patterns of the crushed crystals were collected using an X-ray powder diffractometer (MiniFlex II, Rigaku, Cu Kα, Tokyo, Japan), with the accelerating voltage and the applied current of 40 kV and 40 mA. The diffraction peaks were recorded in a 2θ range of 5–80° with a scan step of $0.033° \cdot s^{-1}$. Elemental analysis of the crystals obtained was conducted by the energy-dispersive X-ray spectroscopy (EDX; Inca Oxford Instruments, Tokyo, Japan) equipped with field emission scanning electron microscopy (SEM; S-3400N, Hitachi, Tokyo, Japan). The single crystal X-ray diffraction data were collected on a diffractometer (XtaLAB Pro, Rigaku, Mo Kα radiation, Tokyo, Japan). The data collections for the structure analysis were carried out using the single crystals with approximate dimensions of $120 \times 80 \times 20$ μm^3 and $340 \times 210 \times 40$ μm^3 for Bi_4NbO_8Cl and $75 \times 60 \times 20$ μm^3 for Bi_4NbO_8Br. The data reductions were carried out using CrysAlisPro (Oxford Diffraction ver. 1.171.39.20a, Rigaku, Tokyo, Japan). The empirical absorption correction was applied using spherical harmonics implemented in SCALE3 ABSPACK scaling algorithm. The structural parameters were refined by full-matrix least-squares on F^2 using *SHELXL*-2016 [21], with the crystallographic data listed in Table S6.

Polarized Raman measurements were performed in a backscattering geometry using an iHR320 monochromator (Horiba, Kyoto, Japan) equipped with an iDUS420 charge-coupled-device camera (Andor, Tokyo, Japan) [22]. Linearly polarized incident light from a diode-pumped solid-state laser (LCX-532S-300, Oxxius, Lannion, France) with single-frequency operation at 532 nm traveled toward the sample through a polarization rotation device (Sigma Koki, Tokyo, Japan) [23] equipped with a broadband half-wave plate (Kogakugiken, Kanagawa, Japan) in the microscope. The elastic stray component below 3 cm^{-1} was suppressed using three ultra-narrowband holographic notch filters (OptiGrate, Oviedo, FL, USA).

4. Conclusions

We investigated crystal growth conditions of Bi_4NbO_8Cl and found that the suppression of volatilization of Bi–O–Cl species is essential. The single-crystal XRD on the platelet crystal revealed that a pseudo-merohedral twin is likely present with domains in the *ab* plane, in addition to the ferroelectric domains. We also report the growth of single crystal Bi_4NbO_8Br for the first time. The successful preparation of these crystals enables various experiments, such as optical measurements under high magnetic field, to be performed in future, offering us possibilities to gain deeper insight into photocatalytic properties of Bi_4NbO_8X. Furthermore, the Sillén–Aurivillius series, with the general formula $[(Bi_2O_2)_2X]^{3+}[A_{n-1}B_nO_{3n+1}]^{3-}$ (n = 1, 2, 3, ...) constitutes a promising material platform not only for the photocatalysis but also for ferroelectric [24] or multiferroic properties [25]. We believe that the knowledge of single crystal growth obtained in this study on Bi_4NbO_8X can be applied to other Sillén–Aurivillius oxyhalide compounds.

Supplementary Materials: The following are available online at http://www.mdpi.com/2304-6740/6/2/41/s1, Figure S1: Powder XRD of obtained product when using reported condition, Figure S2: A picture of obtained product with grey agglomerate and yellow crystalline mass, Figure S3: EDX spectra of (a) Bi_4NbO_8Cl and (b) Bi_4NbO_8Br crystal, Table S1: Refined structural parameters for Bi_4NbO_8Cl at 293 K in the space group $P2_1cn$, Table S2: Selected bond lengths and angles for Bi_4NbO_8Cl. Table S3: Calculated bond valence sum values of Bi_4NbO_8Cl, Figure S4: Polarized Raman spectra of Bi_4NbO_8Cl in cross nicol geometries, Figure S5: Reciprocal lattice plane of Bi_4NbO_8Br. Refined structural parameters for Bi_4NbO_8Br at 293 K in the space group $P2_1cn$, Table S4: Refined structural parameters for Bi_4NbO_8Br at 293 K in the space group $P2_1cn$. Lattice parameters: a = 5.51190(10) Å, b = 5.51190(10) Å, c = 29.0984(14) Å, Table S5: Selected bond lengths and angles for Bi_4NbO_8Br, Table S6: Crystallographic data for Bi_4NbO_8Cl and Bi_4NbO_8Br.

Author Contributions: Chengchao Zhong, Daichi Kato and Hiroshi Kageyama conceived and designed the experiments; Chengchao Zhong performed crystal growth, XRD, EDX-SEM experiments; Kotaro Fujii, Masatomo Yashima and Cédric Tassel contributed single-crystal XRD; Yasuhiro Fujii and Akitoshi Koreeda were responsible for polarized Raman measurement; Emily Nishiwaki and all the members above discussed the results with assistance from Ryu Abe. Chengchao Zhong and Hiroshi Kageyama wrote the paper with assistance mainly from Fumitaka Takeiri.

Conflicts of Interest: The authors declare no conflict of interest.

References

1. Kageyama, H.; Hayashi, K.; Maeda, K.; Attfield, J.P.; Hiroi, Z.; Rondinelli, J.M.; Poeppelmeier, K.R. Expanding frontiers in materials chemistry and physics with multiple anions. *Nat. Commun.* **2018**, *9*, 772. [CrossRef] [PubMed]

2. Atuchin, V.V.; Isaenko, L.I.; Kesler, V.G.; Lin, Z.S.; Molokeev, M.S.; Yelisseyev, A.P.; Zhurkov, S.A. Exploration on anion ordering, optical properties and electronic structure in $K_3WO_3F_3$ elpasolite. *J. Solid State Chem.* **2012**, *187*, 159–164. [CrossRef]

3. Atuchin, V.V.; Molokeev, M.S.; Yurkin, G.Y.; Gavrilova, T.A.; Kesler, V.G.; Laptash, N.M.; Flerov, I.N.; Patrin, G.S. Synthesis, structural, magnetic, and electronic properties of cubic $CsMnMoO_3F_3$ oxyfluoride. *J. Phys. Chem. C* **2012**, *116*, 10162–10170. [CrossRef]

4. Maeda, K.; Takata, T.; Hara, M.; Saito, N.; Inoue, Y.; Kobayashi, H.; Domen, K. GaN: ZnO solid solution as a photocatalyst for visible-light-driven overall water splitting. *J. Am. Chem. Soc.* **2005**, *127*, 8286–8287. [CrossRef] [PubMed]

5. Yashima, M.; Yamada, H.; Maeda, K.; Domen, K. Experimental visualization of covalent bonds and structural disorder in a gallium zinc oxynitride photocatalyst $(Ga_{1-x}Zn_x)(N_{1-x}O_x)$: Origin of visible light absorption. *Chem. Commun.* **2010**, *46*, 2379–2381. [CrossRef] [PubMed]

6. Ishikawa, A.; Takata, T.; Kondo, J.N.; Hara, M.; Kobayashi, H.; Domen, K. Oxysulfide $Sm_2Ti_2S_2O_5$ as a stable photocatalyst for water oxidation and reduction under visible light irradiation ($\lambda \leq 650$ nm). *J. Am. Chem. Soc.* **2002**, *124*, 13547–13553. [CrossRef] [PubMed]

7. Ishikawa, A.; Takata, T.; Matsumura, T.; Kondo, J.N.; Hara, M.; Kobayashi, H.; Domen, K. Oxysulfides $Ln_2Ti_2S_2O_5$ as stable photocatalysts for water oxidation and reduction under visible-light irradiation. *J. Phys. Chem. B* **2004**, *108*, 2637–2642. [CrossRef]

8. Fujito, H.; Kunioku, H.; Kato, D.; Suzuki, H.; Higashi, M.; Kageyama, H.; Abe, R. Layered perovskite oxychloride Bi_4NbO_8Cl: A stable visible light responsive photocatalyst for water splitting. *J. Am. Chem. Soc.* **2016**, *138*, 2082–2085. [CrossRef] [PubMed]

9. Ackerman, J.F. The structures of Bi_3PbWO_8Cl and Bi_4NbO_8Cl and the evolution of the bipox structure series. *J. Solid State Chem.* **1986**, *62*, 92–104. [CrossRef]

10. Kunioku, H.; Higashi, M.; Tomita, O.; Yabuuchi, M.; Kato, D.; Fujito, H.; Kageyama, H.; Abe, R. Strong hybridization between Bi-6s and O-2p orbitals in Sillén–Aurivillius perovskite Bi_4MO_8X (M = Nb, Ta; X = Cl, Br), visible light photocatalysts enabling stable water oxidation. *J. Mater. Chem. A* **2018**, *6*, 3100–3107. [CrossRef]

11. Kato, D.; Hongo, K.; Maezono, R.; Higashi, M.; Kunioku, H.; Yabuuchi, M.; Suzuki, H.; Okajima, H.; Zhong, C.; Nakano, K.; et al. Valence band engineering of layered bismuth oxyhalides toward stable visible-light water splitting: Madelung site potential analysis. *J. Am. Chem. Soc.* **2017**, *139*, 18725–18731. [CrossRef] [PubMed]

12. Silvestri, V.J.; Sedgwick, T.O.; Landermann, J.B. Vapor growth of $Bi_{12}GeO_{20}$, γ-Bi_2O_3 and BiOCl. *J. Cryst. Growth* **1973**, *20*, 165–168. [CrossRef]

13. Peng, H.; Chan, C.K.; Meister, S.; Zhang, X.F.; Cui, Y. Shape evolution of layer-structured bismuth oxychloride nanostructures via low-temperature chemical vapor transport. *Chem. Mater.* **2008**, *21*, 247–252. [CrossRef]

14. Binnewies, M.; Glaum, R.; Schmidt, M.; Schmidt, P. *Chemical Vapor Transport Reactions*; Walter de Gruyter: Berlin, Germany, 2012.

15. Zhao, L.; Zhang, X.; Fan, C.; Liang, Z.; Han, P. First-principles study on the structural, electronic and optical properties of BiOX (X = Cl, Br, I) crystals. *Physica B* **2012**, *407*, 3364–3370. [CrossRef]

16. Kusainova, A.M.; Stefanovich, S.Y.; Dolgikh, V.A.; Mo-sunov, A.V.; Hervoches, C.H.; Lightfoot, P. Dielectric properties and structure of Bi_4NbO_8Cl and Bi_4TaO_8Cl. *J. Mater. Chem.* **2001**, *11*, 1141–1145. [CrossRef]

17. Schneemeyer, L.F.; Waszczak, J.V.; Siegrist, T.; Van Dover, R.B.; Rupp, L.W.; Batlogg, B.; Cava, R.J.; Murphy, D.W. Superconductivity in $YBa_2Cu_3O_7$ single crystals. *Nature* **1987**, *328*, 601. [CrossRef]

18. Ishiguro, T.; Kitazawa, A.; Mizutani, N.; Kato, M. Single-crystal growth and crystal structure refinement of $CuAlO_2$. *J. Solid State Chem.* **1981**, *40*, 170–174. [CrossRef]

19. Kusainova, A.M.; Zhou, W.; Irvine, J.T.; Lightfoot, P. Layered Intergrowth Phases Bi_4MO_8X (X = Cl, M = Ta and X = Br, M = Ta or Nb): Structural and Electrophysical Characterization. *J. Solid State Chem.* **2002**, *166*, 148–157. [CrossRef]

20. He, Y.; Zhang, Y.; Huang, H.; Tian, N.; Guo, Y.; Luo, Y. A novel Bi-based oxybromide Bi_4NbO_8Br: Synthesis, characterization and visible-light-active photocatalytic activity. *Colloid Surf. A Physicochem. Eng. Asp.* **2014**, *462*, 131–136. [CrossRef]

21. Sheldrick, G.M. Crystal structure refinement with *SHELXL*. *Acta Crystallogr. C* **2015**, *71*, 3–8. [CrossRef] [PubMed]

22. Fujii, Y.; Katayama, D.; Koreeda, A. Broadband light scattering spectroscopy utilizing an ultra-narrowband holographic notch filter. *Jpn. J. Appl. Phys.* **2016**, *55*, 10TC03. [CrossRef]

23. Fujii, Y.; Noju, M.; Shimizu, T.; Taniguchi, H.; Itoh, M.; Nishio, I. Raman tensor analysis of crystalline lead titanate by quantitative polarized spectroscopy. *Ferroelectrics* **2014**, *462*, 8–13. [CrossRef]

24. Kusainova, A.M.; Lightfoot, P.; Zhou, W.; Stefanovich, S.Y.; Mosunov, A.V.; Dolgikh, V.A. Ferroelectric properties and crystal structure of the layered intergrowth phase $Bi_3Pb_2Nb_2O_{11}Cl$. *Chem. Mater.* **2001**, *13*, 4731–4737. [CrossRef]

25. Liu, S.; Miiller, W.; Liu, Y.; Avdeev, M.; Ling, C.D. Sillen–Aurivillius intergrowth phases as templates for naturally layered multiferroics. *Chem. Mater.* **2012**, *24*, 3932–3942. [CrossRef]